# Topological Analysis of Charge Density Distribution in Concomitant Polymorphs of 3-Acetylcoumarin, A Case of Packing Polymorphism

**2 AUTHORS**, INCLUDING:

Parthapratim Munshi

Shiv Nadar University

**42** PUBLICATIONS    **659** CITATIONS

SEE PROFILE

# Topological Analysis of Charge Density Distribution in Concomitant Polymorphs of 3-Acetylcoumarin, A Case of Packing Polymorphism

Parthapratim Munshi and Tayur N. Guru Row*

*Solid State and Structural Chemistry Unit, Indian Institute of Science, Bangalore-560012, India*

**ABSTRACT:** Detailed investigation of the charge density distribution in concomitant polymorphs of 3-acetylcoumarin in terms of experimental and theoretical densities shows significant differences in the intermolecular features when analyzed based on the topological properties via the quantum theory of atoms in molecules. The two forms, triclinic and monoclinic (Form A and Form B), pack in the crystal lattice via weak C−H···O and C−H···$\pi$ interactions. Form A results in a head-to-head molecular stack, while Form B generates a head-to-tail stack. Form A crystallizes in $P\bar{1}$ ($Z' = 2$) and Form B crystallizes in $P2_1/n$ ($Z' = 1$). The electron density maps of the polymorphs demonstrate the differences in the nature of the charge density distribution in general. The charges derived from experimental and theoretical analysis show significant differences with respect to the polymorphic forms. The molecular dipole moments differ significantly for the two forms. The lattice energies evaluated at the HF and DFT (B3LYP) methods with 6-31G** basis set for the two forms clearly suggest that Form A is the thermodynamically stable form as compared to Form B. Mapping of electrostatic potential over the molecular surface shows dominant variations in the electronegative region, which bring out the differences between the two forms.

## Introduction

Polymorphism in molecular crystals has received considerable attention in recent years particularly from the point of view of "drug design",[1,2] which demands an unequivocal characterization of all possible crystalline forms of a drug material. It is in this context that the studies of concomitant polymorphism (in which crystallization occurs simultaneously from the same solvent and in the same crystallizing flask under identical crystal growth conditions) in a given material gains paramount significance. In general, polymorphs are classified into three major categories based on the geometry of molecular assembly in the crystal lattice. Of these, conformational polymorphism, which involves changes at the molecular level, occurs predominantly in flexible molecules. In the case of rigid molecules, the differences occur mainly in the packing motifs directed by the intermolecular interactions, which results in packing polymorphism. The third category is a consequence of the presence of solvent molecules in the crystal lattice, referred to as pseudo or solvato-morphism, which involves large changes in crystal density and packing. A significant number of molecules exhibit polymorphism, as can be seen from an analysis of the entries in the Cambridge Structural Database (CSD).[3] In the recent literature, several careful studies have been made to evaluate the role of the solvent in the formation of polymorphism. These highlight the importance of the kinetics in solution rather than the formation of molecular assemblies.[4] In the case in which specific thermodynamic conditions result in a crystallization process, which has nearly similar rates in kinetics, two or more polymorphs may appear resulting in the phenomenon of concomitant polymorphism.[2,5] The nearly equivalent crystal energetics involved in the generation of concomitant polymorphs provides excellent and demanding benchmarks for theoretical and computational models.[6] One of the important questions that arises is to understand the energetics involved in concomitant polymorphism on the basis of the specific intermolecular interactions.

Determination of the lattice energy in the vicinity of the molecule, either by appropriate computational (theoretical) methods or by careful analysis of the charge density distribution via accurate experimental measurements, may provide the appropriate answer.

Charge density analysis is an attractive tool to study a wide range of problems of physical and chemical interest.[7] All ground-state properties are unique functionals of the charge density based on the Hohenberg−Kohn theorem,[8] which provides pointers to the importance of charge density features in molecular crystals. An understanding of the phenomena of polymorphism in terms of charge density distributions has received some interest in recent times[9−12] with the realization that geometrical arrangements in crystal lattices are significantly guided by thermodynamic and kinetic factors. In literature, the study of polymorphic structures from the charge density point of view are rare with only one experimental electron density study on two markedly different molecular conformations of famotidine[9] and two other cases of packing polymorphs, one on *p*-nitrophenol[10] and the other on 5-nitrouracil.[11] There is just one example of an inorganic polymorph [antimony (III) oxide] studied via charge density analysis.[12] In the case of packing polymorphism, the contribution to the difference in the total lattice energy arises mainly from intermolecular interactions, and such values can only be quantitatively evaluated either from experimental or theoretical charge densities. The appearance of concomitant polymorphs presents an ideal case for charge density analysis since the conclusions based on electrostatic potentials, lattice energies, and interaction pathways could provide insights into the subtle interplay between the thermodynamic and the kinetic factors.

Here we report the first case study of concomitant polymorphism in 3-acetylcoumarin in terms of the topological analysis of charge densities derived from both experimental and theoretical studies. 3-Acetylcoumarin crystallizes concomitantly in two forms as earlier reported by us,[13] and the intermolecular interactions are essentially C−H···O and C−H···$\pi$, which are responsible for arranging a head-to-head stacking in Form A and a head-to-tail stacking in Form B. Interestingly, Form A provides an opportunity to study a system with two crystallo-

* To whom correspondence should be addressed. Professor T. N. Guru Row, Solid State and Structural Chemistry Unit, Indian Institute of Science, Bangalore − 560012, India. Tel: +91-80-22932796. Fax: +91-80-23601310. E-mail: ssctng@sscu.iisc.ernet.in.

graphically independent molecules [$Z' = 2$, molecule 1 and molecule 2]. Indeed, electron density studies of such systems are sparse,[14−16] and in the context of the present study of concomitant polymorphism, provides yet another variant with the presence of two molecules exposed to dissimilar crystal fields. Also it is noteworthy that this study is unique since it offers a study related to (a) two molecules in the asymmetric unit exhibiting conformational differences and (b) packing polymorphism involving only weak intermolecular interactions. Mapping of the charge density distribution in the two remarkably different packing motifs is expected to provide the details of the energetics in directing the molecular assembly in these concomitant polymorphs.

An accurate experimental measurement and analysis of charge density in a molecular crystal can be obtained from high-resolution X-ray diffraction data at low temperatures.[17] Hansen and Coppens formalism[18] is a widely used approach in which the individual atomic densities are divided into three components as given below

$$\rho_{at}(\mathbf{r}) = P_c\rho_{core}(\mathbf{r}) + P_v\kappa^3\rho_{valenc}(\kappa\mathbf{r}) + $$
$$\sum_{l=0}^{l_{max}}\kappa'^3 R_l(\kappa'\mathbf{r}) \sum_{m=0}^{l} P_{lm}\pm d_{lm}\pm(\vartheta,\varphi)$$

and the electron density in the crystal is modeled based on this $\rho_{at}(\mathbf{r})$ as a sum of atom-centered charge distributions. Interpretation of the charge density as obtained from experimental electron density can be done using Bader's quantum theory of atoms in molecules (AIM) approach.[19] It also provides a pathway for comparing the experimental electron density with the theoretically derived density in terms of topological properties of the electron density $\rho(\mathbf{r})$. The line of the highest electron density linking any two atoms is referred to as the "bond path" (BP) and its length $R_{ij}$ (need not be the same as interatomic vector) is referred to as the "interaction line". The bond critical points (BCPs) lie along the bond path with the gradient of the electron density, $\Delta\rho_b(\mathbf{r}) = 0$. The second derivative of the electron density, the Laplacian $\nabla^2\rho_b(\mathbf{r})$ ($= \sum_{i=1}^{3} \lambda_i$, $\lambda_i$ are the curvatures of a bond at the BCP), represents the chemical features of the molecules. If $\nabla^2\rho_b(\mathbf{r}) < 0$, the density is locally concentrated resulting in shared interactions, while in the case of $\nabla^2\rho_b(\mathbf{r}) > 0$ the electron density is depleted representing closed-shell interactions. Further, the degree of aromaticity in a particular chemical bond is represented by bond ellipticity, $\epsilon = (\lambda_1/\lambda_2) - 1$. The electron density, Laplacian, interaction line, the curvatures, and the bond ellipticity together represent the topology of the charge density distribution in a given molecule. To characterize a bond in terms of its chemical concepts such as bond order, ionicity conjugation, and hydrogen bonding the properties evaluated at the BCPs become crucial. Koch and Popelier (here after referred to as KP) have proposed eight criteria to establish hydrogen bonding in particular, which allows one to distinguish a hydrogen bond from a van der Waals interaction.[20] A recent study by us[16] suggests the use of such criteria to derive features related to the limit of a hydrogen bond in molecular crystals, thus forming a basis for quantitative crystal engineering. In this article, charge density features to distinguish between two concomitant packing polymorphs are derived for the first time restricting to the first four criteria to quantify intermolecular interactions. The presence of a BCP between a donor atom and an acceptor atom linked via a bond path forms the basis of the first condition. The second condition tells about the charge density evaluated at the BCP and its relationship with the overall hydrogen bond energy. It is possible to

relate[9,5,10] the charge density parameters at the BCP to the local electronic kinetic energy density, $G(\mathbf{r}_{CP})$ and the local potential energy density, $V(\mathbf{r}_{CP})$ and hence the total local energy density, $E(\mathbf{r}_{CP})$. The third condition refers to the positive values of the Laplacian at the BCP, $\nabla^2\rho_b(\mathbf{r})$ and should correlate with the interaction energies. The fourth condition deals with the mutual penetration of the hydrogen and the acceptor atom. This condition, considered as necessary and sufficient, compares the nonbonded radii of the donor hydrogen atom ($r_D^0$) and the acceptor atom ($r_A^0$) with their corresponding bonding radii. The nonbonding radius is taken to be equivalent to the gas-phase van der Waals radius of the participating atoms.[21] The bonding radius ($r$) is the distance from the nucleus to the BCP. In a typical hydrogen bond, the value of $\Delta r_D = (r_D^0 - r_D) > \Delta r_A = (r_A^0 - r_A)$ and $\Delta r_D + \Delta r_A > 0$ represent positive interpenetration. If either or both of these conditions are violated, the interaction is essentially van der Waals in nature.

## Experimental Section

3-Acetylcoumarin (IUPAC name: 3-acetyl-2H-1-benzopyran-2-one) was synthesized according to the reported procedure.[22] It was obtained by reacting an equimolar proportion of ethylacetoacetate and salicylaldehyde in the presence of piperidine as catalyst at cold temperature. The product was washed with ethanol and recrystallized by glacial acetic acid at room temperature (∼23 °C). The purified compound was obtained in satisfactory yield (96%). Concomitant crystals were grown as described earlier, and the existence of two polymorphs, prismatic form (Form A) and needle form (Form B), were confirmed in terms of powder X-ray diffraction patterns, differential scanning calorimetry, infrared spectroscopy, and finally single-crystal X-ray diffraction (SXRD).[13]

The high-resolution SXRD data were collected on a Bruker AXS SMART APEX CCD diffractometer using MoK$_\alpha$ radiation (50 kV, 40 mA). To achieve the final temperature, the ramp rate was set to 40 K/h. During the data collection, the temperature was maintained at 90.0-(2) K by using the Oxford Cryo systems with N$_2$ flows. Suitable crystals with reasonable sizes (Table 1) were mounted in a Lindeman capillary and allowed to stabilize at final temperature for an hour. The unit-cell parameters were determined repeatedly until the estimated standard deviations in cell dimensions did not vary beyond acceptable limits. The data were collected in three steps with different scan times (15, 55, and 105 s for Form A, while 20, 45, and 100 s for Form B) to

**Table 1. Experimental Single-Crystal X-ray Diffraction Data**

| compound | Form A[13] | Form B |
|---|---|---|
| formula | C$_{11}$H$_8$O$_3$ | C$_{11}$H$_8$O$_3$ |
| crystal sizes | 0.46 × 0.29 × 0.25 | 0.38 × 0.26 × 0.07 |
| formula weight | 188.17 | 188.17 |
| space group | $P\bar{1}$ | $P2_1/n$ |
| temperature/K | 90.0(2) | 90.0(2) |
| unit cell dimensions/Å | | |
| $a$ | 7.4772(15) | 11.3068(7) |
| $b$ | 9.6304(19) | 3.9871(2) |
| $c$ | 11.989(2) | 18.7586(11) |
| $\alpha$/° | 85.751(11) | 90.00 |
| $\beta$/° | 86.099(11) | 90.454(2) |
| $\gamma$/° | 81.753(11) | 90.00 |
| $V$/Å$^3$ | 850.6(3) | 845.64(8) |
| $Z, D_c$/g cm$^{-3}$ | 4, 1.469 | 4, 1.478 |
| $F(000)$ | 392 | 392 |
| absorption coeff/mm$^{-1}$ | 0.107 | 0.108 |
| radiation | MoK$_\alpha$ | MoK$_\alpha$ |
| $(\sin\theta/\lambda)_{max}$/Å$^{-1}$ | 1.08 | 1.08 |
| $R$(merge) | 0.0182 | 0.0243 |
| reflection nos. (unique) | 12716 | 6581 |
| $R(F)$ | 0.0196 | 0.0209 |
| $R_w(F), S$ | 0.0192, 1.96 | 0.0186, 2.07 |
| $N_{obs}/N_{par}$ | 12.71 | 12.95 |
| range of residual density/e Å$^{-3}$ | −0.198, 0.219 | −0.223, 0.246 |

cover the full-sphere of reciprocal space with different $2\theta$ settings of the detector ($-25°$, $-50°$, and $-75°$) and $\varphi$ settings ($0°$, $90°$, $180°$, and $270°$) of the goniometer and the scanning angle $\omega$ was set to $0.3°$ for each 606 frames. An additional 60 frames were collected with $2\theta$ settings of the detector at $-25°$ and $\varphi$ settings at $0°$ at the end of the data collection to perform the crystal decay correction. The crystal-to-detector distance was kept at 6.03 cm. This strategy[23] provides high resolution, large redundancy, and appropriate completeness in data sets, which are the key factors for multipole refinement modeling. The data collection was monitored and reduced with the packages SMART[24] and SAINTPLUS,[24] respectively. Sorting, scaling, merging, and empirical correction for absorption of the set of intensities were performed with SORTAV.[25] The structures were solved by direct methods using SHELXS97[26] and refined in the spherical atom approximation (based on $F^2$) by using SHELXL97[25] included in a complete package WinGX.[27] The molecular diagrams were generated using ORTEP-3[28] and the geometrical analysis were performed by PARST95.[29]

**Multipole Refinement.** The package XD[30] was used to perform the detail analysis of charge density distribution in the two polymorphic forms. The module XDLSM,[30] which is a full-matrix least squares program, was used to carry out the multipolar refinement. The residual bonding density, not modeled in the conventional spherical refinement, is taken into account in this multipolar refinement. Scattering factors were derived from the Clementi and Roetti[31] wave functions for all atoms. The function minimized in the least-squares refinement is $\Sigma w(|F_0|^2 - K|F_c|^2)^2$ for all reflections with $I > 3\sigma(I)$. A similar refinement procedure as described earlier by us[16,23] was followed for both forms. Initially, only the scale factor was refined with all reflections. Next, to determine the accurate positional and thermal parameters, the higher order ($\sin \theta/\lambda \geq 0.8$ Å$^{-1}$) refinements were performed for non-H atoms. The positional and isotropic thermal parameters of the H atoms were then refined using the lower angle data ($\sin \theta/\lambda \leq 0.8$ Å$^{-1}$). Because of the unavailability of the neutron data the positions of the H atoms in this refinement as well as in the subsequent refinements were fixed to average bond distance values obtained from reported neutron diffraction studies.[32] In the next stage monopole, dipole, quadrupole, octapole, and hexadecapole populations were allowed to refine in a stepwise manner. Next, only single $\kappa$ parameters and then single $\kappa'$ parameters together with $\kappa$ for all non-H atoms were refined. Finally, all the multipole parameters (including the isotropic thermal parameters of H atoms) were refined to reach the final model of charge density distribution. For all H atoms the multipole expansion was truncated at the $l_{max} = 1$ (dipole, bond-directed) level. For chemically different groups of non-hydrogen atoms separate $\kappa$ and $\kappa'$ were allowed while for H atoms the corresponding values were fixed at 1.2. No chemical restraints were applied, but the molecular electro-neutrality constraint was applied and the scale factor was allowed to refine throughout all refinements. The modules XDFFT[30] and XDFOUR[30] were used to measure the amount of residual electron density and dynamic deformation density and hence confirmed the refinement procedure. The module XDPROP[30] of the package XD was used for topological analysis of the electron densities.

The intermolecular interaction energies can be calculated from the experimental charge density approach by using the program XDINTER.[33] The calculation provides the binding energy in terms of the electrostatic, exchange-repulsion, and dispersion components. The anisotropic electrostatic interaction energy was derived from atom-centered multipoles,[7] while the exchange-repulsion and dispersion energies were calculated based on Spackman's exp-6 atom–atom potentials.[34] The corresponding lattice energies were estimated by subtracting the relaxation energies (obtained from GAUSSIAN98[35] described later) from the value of the binding energies.[33,36]

## Theoretical Calculations

**Calculation of Periodic Wave function and Theoretical Structure Factors.** The program CRYSTAL03[37] was used to perform the single-point periodic calculations based on the experimental geometry by using density functional theory (DFT) method at the B3LYP[38] level with the 6-31G** basis set.[39] This basis set has been shown to provide reliable and consistent results with respect to studies involving intermolecular interactions.[16,40] The shrinking factors (IS1, IS2, and IS3) along the

reciprocal lattice vectors were set at 4 (30 K-points in the irreducible Brillouin zone). For all the three compounds, the truncation parameters (ITOL), which control the accuracy of the calculation of the bielectronic Coulomb and exchange series, were set as ITOL1 = ITOL2 = ITOL3 = ITOL4 = 6 and ITOL5 = 15. As suggested by Spackman and Mitchell,[41] the exponents of the polarization functions were not scaled due to the large difference between ITOL4 and ITOL5. Rapid convergence was achieved when the level shifter value was set equal to 0.3 Hartree. Upon convergence on energy ($\sim10^{-6}$) the periodic wave function was obtained and used to generate the static theoretical structure factors with the option XFAC. It may be mentioned that calculations at the Hartree–Fock (HF) level using the same basis set were performed but are not included in the rest of the discussion since the electron correlation is not included in such calculations.

To eliminate an important source of correlation between parameters, the temperature factors and atomic positions were not refined during the multipole refinement of the static theoretical structure factors via XD. The same multipoles, as used in the refinement of experimental structure factors, were allowed to refine with separate $\kappa'$ parameters for each non-H atom. All the theoretical reflections were included in the refinements.

The lattice energies were calculated based on the procedure[36] described by Abramov et al., which defines the lattice energy as the difference between the molecular interaction energy in the crystal and the molecular relaxation energy upon sublimation. The molecular interaction energy was evaluated as the difference between the energy of the molecule in the crystal to that of the isolated molecule with the crystal geometry. The package CRYSTAL03 was used to obtain the molecular interaction energy after correcting for basis set superposition error by adopting the counterpoise method.[42] Relaxation energy was obtained as the difference between the energy of the isolated molecule with optimized geometry and the molecule with crystal geometry. This energy calculation was performed at the HF and B3LYP levels with the 6-31G** basis set via GAUSSIAN98.

## Results and Discussion

Table 1 list the unit cell parameters, the experimental details, and the parameters from multipole refinement of SXRD data for Form A and Form B. Figure 1 gives the molecular ORTEP with 50% probability for non-H atoms in both forms, showing the atom labeling for two molecules in the asymmetric unit in Form A and only one molecule in Form B. In our earlier report,[13] the differences in the conformation at the acetyl group in both Form A and Form B and also the occurrence of intermolecular C–H$\cdots$O and C–H$\cdots\pi$ interactions have been highlighted. In addition, in Form A the dihedral angle between the plane of the acetyl-group (C2–C10–C11–O3) and the plane through the carbon atoms of the basic coumarin moiety (C1–C9) rings is 8.93(2)° (molecule 1) and 4.74(2)° (molecule 2), respectively, while in Form B the angle is 6.81(1)°.

**Charge Density Analysis.** Hirshfeld's rigid bond test[43] was applied during the final refinement for intramolecular bonds, not involving H atoms. The maximum differences of mean-squares displacement amplitudes values were found to be $6 \times 10^{-4}$ Å$^2$ for the bonds C(4)–C(9) and C(3)–C(9) in molecule 1 (Form A), C(2A)–C(10A) in molecule 2 (Form A) and C(4)–C(9) and C(10)–C(11) (Form B), indicating that the atomic thermal vibrations are properly accounted for.

The residual densities (Supporting Information, Figure S1) in Form A lie between $-0.183$ to $0.207$ eÅ$^{-3}$ (concentrated in
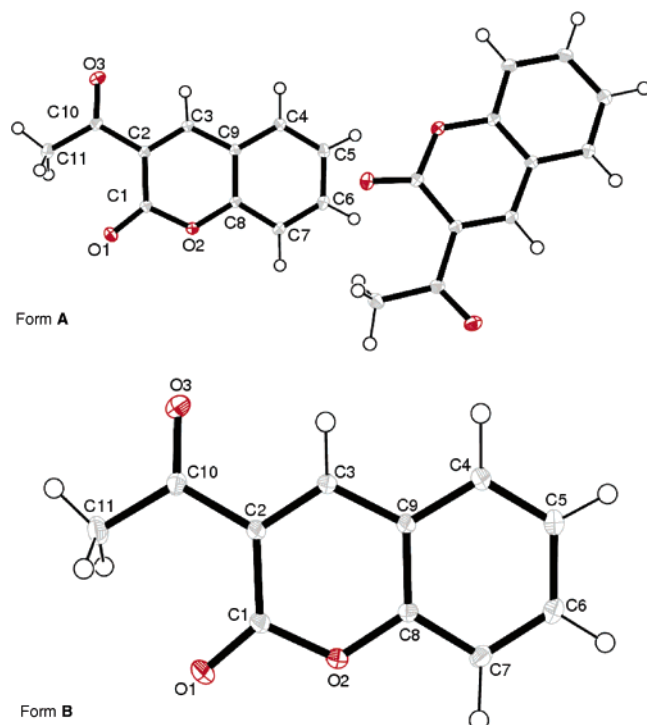
**Figure 1.** ORTEP diagram with labels for atoms of 3-acetylcoumarin at 90 K with 50% ellipsoid probability for non-H atoms.

the bonding regions) for molecule 1 and −0.159 to 0.206 e$Å^{-3}$ (localized at atom sites and ring centers) for molecule 2. For Form B the corresponding values are −0.209 to 0.252 e $Å^{-3}$ concentrated at the ring centers. These values and the maps are in agreement with the reported studies on related structures.[44,45] The minimum and the maximum residual densities over the entire asymmetric unit as listed in Table 1 depict the correctness of the model. The corresponding dynamic deformation density maps (Supporting Information, Figure S2) show essentially similar features of bonding density. The static maps (devoid of thermal smearing) obtained from multipole analysis of both experimental and theoretical structure factors are in reasonable agreement as can be seen from Figure 2. The lone pair of electrons on the O atoms is prominently seen in both forms in general. However, in both forms a depletion of charge density along the bonds connecting the O atom in the ring is indicated in the experimental maps and appears more prominently in the theoretical maps (Figure 2). It is noteworthy that the appearance of fewer contours around the H atoms in Form B is mainly a consequence of the conformational differences between the two forms rather than any deficiency in the quality of the data and the multipole model.

Table S2 (Supporting Information) gives the relevant intramolecular bond properties for non-H atoms in both forms, and the following general observations can be deduced from these values. Significant differences are observed with respect to the bonds involving O atoms. The experimental $\rho_b(\mathbf{r})$ values of Form B are higher than that of Form A [except for the O(3)−C(10) bond]. The BCPs are away from O atoms, and the distances are slightly higher for Form B [except for the O(2)−C(8) bond]. The values of $\epsilon$ are comparable except for the O(3)−C(10) bond (Form B), which is more cylindrical in nature. The comparison of values from the experiment and theory show the following trend: the experimental values of $\rho_b(\mathbf{r})$, $\nabla^2\rho_b(\mathbf{r})$ [except for the O(2)−C(1) bond], and $\epsilon$ for C−O bonds are higher, and the BCPs are slightly closer to the O atoms. However, the corresponding properties of the C−C bonds

**Table 2. Pseudo-Atomic Monopole Charges along with the Bader Charges (Obtained by Integration over the Atomic Basin) Derived from Experiment and Theory[a]**

| | pseudo-atomic monopole charges | | | Bader charges | | |
|---|---|---|---|---|---|---|
| | Form A | | | Form A | | |
| atoms | molecule 1 | molecule 2 | Form B | molecule 1 | molecule 2 | Form B |
| O(1) | −0.58 | −0.62 | −0.50 | −1.29 | −1.30 | −1.40 |
| | −0.13 | −0.13 | −0.13 | −1.11 | −1.09 | −1.12 |
| O(2) | −0.46 | −0.48 | −0.48 | −1.05 | −1.04 | −1.14 |
| | −0.08 | −0.10 | −0.21 | −1.05 | −0.92 | −1.01 |
| O(3) | −0.51 | −0.58 | −0.49 | −1.10 | −1.25 | −1.19 |
| | −0.12 | −0.13 | −0.18 | −1.01 | −0.99 | −1.07 |
| C(1) | 0.22 | 0.15 | 0.09 | 1.36 | 1.28 | 1.35 |
| | −0.11 | −0.09 | −0.08 | 1.27 | 1.32 | 1.32 |
| C(2) | 0.03 | −0.10 | 0.13 | −0.00 | −0.13 | 0.06 |
| | 0.07 | −0.06 | 0.05 | 0.04 | −0.10 | 0.01 |
| C(3) | 0.09 | 0.07 | −0.01 | 0.11 | 0.09 | 0.06 |
| | −0.10 | −0.03 | −0.19 | −0.01 | 0.07 | −0.07 |
| C(4) | −0.04 | 0.03 | 0.029 | −0.05 | 0.01 | 0.03 |
| | −0.13 | −0.07 | −0.14 | −0.04 | 0.03 | −0.04 |
| C(5) | −0.15 | −0.04 | −0.16 | −0.13 | −0.03 | −0.10 |
| | −0.08 | −0.19 | −0.13 | 0.02 | −0.09 | −0.04 |
| C(6) | −0.02 | −0.02 | 0.09 | −0.01 | 0.01 | 0.11 |
| | −0.13 | −0.02 | −0.06 | −0.06 | 0.05 | 0.05 |
| C(7) | −0.02 | 0.07 | 0.04 | −0.07 | 0.00 | 0.01 |
| | −0.13 | −0.12 | −0.18 | −0.04 | −0.03 | −0.09 |
| C(8) | 0.06 | 0.03 | 0.05 | 0.43 | 0.39 | 0.46 |
| | 0.00 | −0.03 | −0.01 | 0.39 | 0.33 | 0.35 |
| C(9) | 0.05 | 0.06 | 0.05 | 0.03 | 0.05 | 0.05 |
| | −0.04 | −0.04 | 0.00 | −0.06 | −0.05 | −0.01 |
| C(10) | 0.35 | 0.31 | 0.23 | 1.00 | 0.89 | 0.96 |
| | −0.04 | 0.02 | −0.02 | 0.85 | 0.90 | 0.90 |
| C(11) | 0.46 | 0.55 | −0.04 | 0.31 | 0.49 | 0.07 |
| | −0.36 | −0.40 | −0.16 | −0.02 | −0.07 | 0.13 |
| H(3) | 0.15 | 0.09 | 0.21 | 0.14 | 0.07 | 0.14 |
| | 0.21 | 0.17 | 0.29 | 0.13 | 0.09 | 0.11 |
| H(4) | 0.07 | 0.07 | 0.04 | 0.07 | 0.07 | 0.03 |
| | 0.18 | 0.17 | 0.20 | 0.11 | 0.08 | 0.11 |
| H(5) | 0.12 | 0.05 | 0.08 | 0.12 | 0.02 | 0.02 |
| | 0.18 | 0.19 | 0.16 | 0.10 | 0.11 | 0.07 |
| H(6) | 0.13 | 0.12 | 0.13 | 0.13 | 0.11 | 0.12 |
| | 0.20 | 0.18 | 0.19 | 0.11 | 0.09 | 0.10 |
| H(7) | 0.21 | 0.15 | 0.18 | 0.24 | 0.18 | 0.15 |
| | 0.14 | 0.14 | 0.18 | 0.06 | 0.07 | 0.09 |
| H(8) | 0.32 | −0.13 | 0.11 | 0.09 | 0.00 | 0.08 |
| | 0.19 | 0.17 | 0.18 | 0.07 | 0.06 | 0.08 |
| H(9) | −0.16 | −0.31 | 0.06 | −0.06 | −0.18 | 0.02 |
| | 0.14 | 0.16 | 0.17 | 0.03 | 0.05 | 0.06 |
| H(10) | −0.13 | 0.35 | 0.17 | −0.01 | 0.02 | 0.09 |
| | 0.18 | 0.20 | 0.16 | 0.06 | 0.09 | 0.06 |

[a] The values from periodic calculation using the B3LYP/6-31G** method are given in italics.

(except for a few cases) from experiment and theory are comparable, and the BCPs are almost at the center of the respective bonds. The $\rho_b(\mathbf{r})$ of the C−C bonds vary within average values of 2.03 e $Å^{-3}$ (experiment), 2.02 e $Å^{-3}$ (theory) for molecule 1 and 2.04 e $Å^{-3}$ (experiment), 2.01 e $Å^{-3}$ (theory) for molecule 2 of Form A and 2.09 e $Å^{-3}$ (experiment), 2.02 e $Å^{-3}$ (theory) for Form B.

The net charges (pseudo-atomic monopole charge) on individual atoms in both Form A and Form B were calculated using the module XDPROP for both experimental and theoretical model densities. The atomic charges (Bader charge) were also deduced based on the integration within the atomic basins as defined by the zero flux surfaces from the multipole models using the program TOPXD.[30] Table 2 compares the values obtained for each atom from these two methods. The monopole charges on O atoms are nearly similar in both forms; however, the experimental values are of higher magnitude than the corresponding charges obtained from theory. The charges on C atoms from the experiment and theory are significantly different,
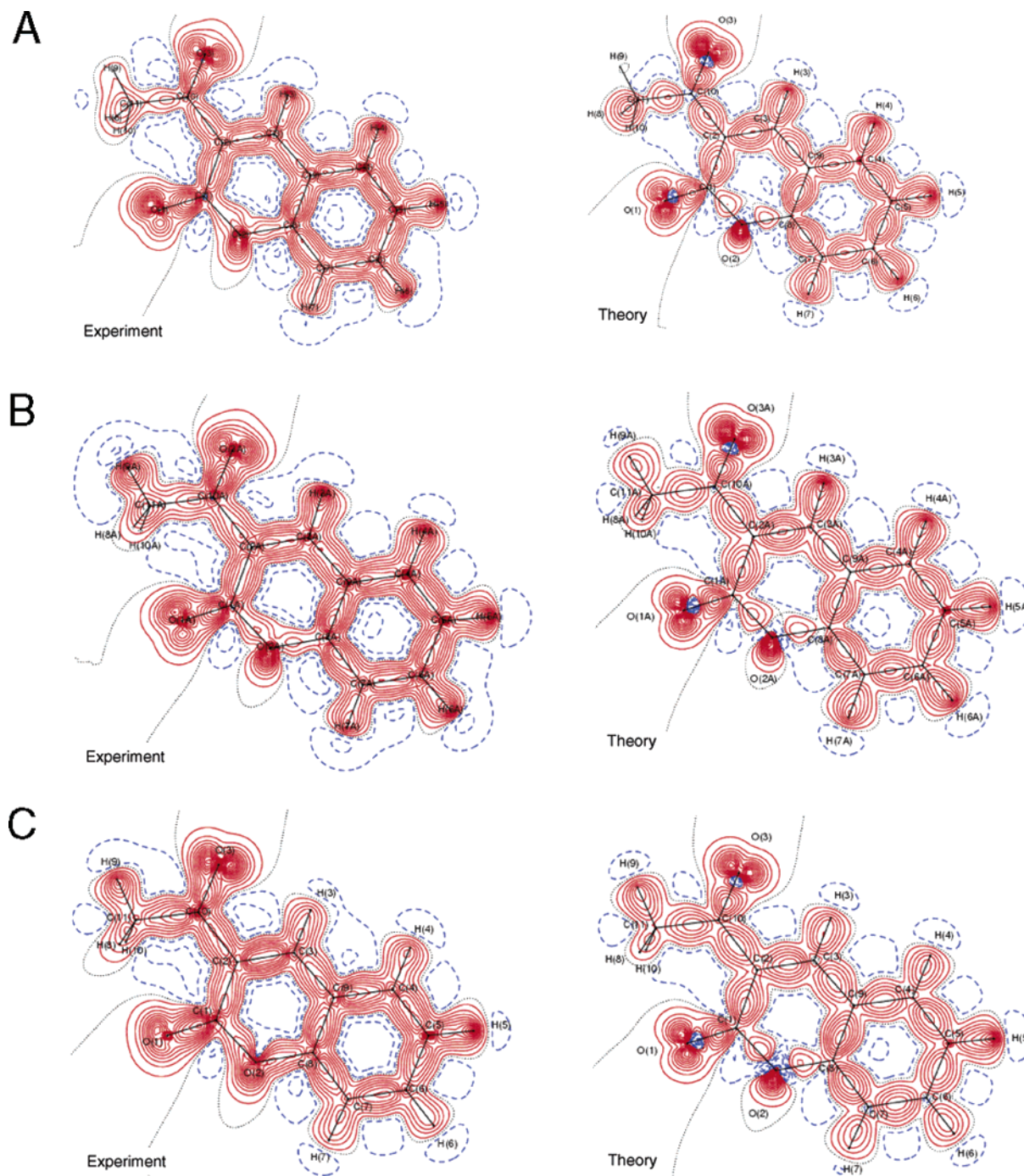
**Figure 2.** (A) Static deformation density map for molecule 1 in Form A. For all static deformation density maps the positive (solids red lines) and negative (broken blue lines) contour starts at ±0.05 e Å$^{-3}$ and with the intervals of ±0.1 e Å$^{-3}$, contour at zero is shown as a black dotted line. (B) Static deformation density map for molecule 2 in Form A. (C) Static deformation density map for Form B.

suggesting that the two forms differ from each other. The experimental and theoretical Bader charges of the O atoms and the connecting C atoms are comparable in both forms but higher in magnitude than the corresponding monopole charges. The $-CH_3$ groups in both forms are easily distinguishable in terms of the experimental values of the atomic monopole charges (higher in magnitude) and Bader charges. On the other hand, the charges on aromatic H atoms are almost similar in each case. The experimental charge density study on the anti-ulcer drug famotidine demonstrates similar results.[9]

Molecular dipole moment is a property that can be of considerable significance in the context of polymorphism. During recent years, it has been recognized that a large and highly significant molecular dipole enhancement may occur upon crystallization, despite the lack of a strongly hydrogen-bonded environment in the crystal.[46] Indeed, the trend followed in the two forms agrees with this observation. Form A has two molecules in the asymmetric unit (hereafter referred to as dimer) and the value of the dipole moment upon crystallization of the dimer is 18.0(16) D (experiment, XD). The corresponding value for Form B (hereafter referred to as monomer) is 9.7(6) D (experiment), which is significantly smaller than that of Form A. The dipole moment values upon geometry optimization of the dimer and the monomer are 7.5 and 4.3 D, respectively.

The packing features of the constituent molecules mainly bring out the difference between the two polymorphic forms.[13]

**Table 3. Intermolecular BCPs and the Parameters Characterizing the Interactions[a]**

| interactions | $R_{ij}$ | $\Delta r_D - \Delta r_A$ | $\Delta r_D + \Delta r_A$ | $\rho_b(\mathbf{r})$ | $\nabla^2\rho_b(\mathbf{r})$ | $G(\mathbf{r}_{CP})$ | $V(\mathbf{r}_{CP})$ |
|---|---|---|---|---|---|---|---|
| | | | Form A | | | | |
| H(6)···O(2A) | 2.421 | 0.130 | 0.319 | 0.049 | 0.953 | 19.36 | −12.76 |
| *(x − 1, y − 1, z)* | *2.397* | *0.135* | *0.343* | *0.047* | *0.947* | *19.11* | *−12.43* |
| H(5A)···O(1A) | 2.426 | 0.230 | 0.314 | 0.032 | 0.995 | 19.08 | −11.05 |
| *(x, y − 1, z)* | *2.420* | *0.175* | *0.320* | *0.038* | *0.879* | *17.30* | *−10.67* |
| H(6A)···O(2) | 2.464 | 0.118 | 0.276 | 0.044 | 0.863 | 17.39 | −11.27 |
| *(x + 1, y, z)* | *2.424* | *0.103* | *0.316* | *0.048* | *0.911* | *18.52* | *−12.24* |
| H(5)···O(1) | 2.472 | 0.239 | 0.268 | 0.030 | 0.876 | 16.81 | −9.77 |
| *(x, y − 1, z)* | *2.429* | *0.155* | *0.311* | *0.041* | *0.869* | *17.30* | *−10.94* |
| H(4A)···O(3) | 2.522 | 0.171 | 0.218 | 0.031 | 0.730 | 14.21 | −8.54 |
| *(x, y, z + 1)* | *2.533* | *0.169* | *0.207* | *0.031* | *0.691* | *13.5* | *−8.19* |
| H(4)···O(3A) | 2.543 | 0.151 | 0.198 | 0.034 | 0.719 | 14.17 | −8.76 |
| *(x, y − 1, z − 1)* | *2.545* | *0.143* | *0.195* | *0.033* | *0.669* | *13.21* | *−8.2* |
| H(7A)···O(1) | 2.65 | 0.222 | 0.090 | 0.021 | 0.567 | 10.8 | −6.15 |
| *(x + 1, y, z)* | *2.636* | *0.099* | *0.104* | *0.033* | *0.598* | *11.92* | *−7.55* |
| H(7)···O(1A) | 2.657 | 0.189 | 0.083 | 0.025 | 0.544 | 10.55 | −6.28 |
| *(x − 1, y − 1, z)* | *2.658* | *0.098* | *0.082* | *0.031* | *0.566* | *11.23* | *−7.05* |
| H(6A)···C(5) | 3.174 | −0.230 | −0.124 | 0.011 | 0.197 | 3.75 | −2.13 |
| *(−x + 1, −y, −z)* | *3.162* | *−0.328* | *−0.112* | *0.016* | *0.223* | *4.37* | *−2.66* |
| H(6A)···C(4) | 3.177 | −0.198 | −0.127 | 0.014 | 0.248 | 4.76 | −2.76 |
| *(−x + 1, −y, −z)* | *3.158* | *−0.338* | *−0.108* | *0.017* | *0.234* | *4.60* | *−2.83* |
| H(4A)···C(3A) | 3.189 | −0.319 | −0.139 | 0.013 | 0.220 | 4.22 | −2.45 |
| *(−x + 1, −y + 1, −z + 1)* | *3.189* | *−0.319* | *−0.139* | *0.012* | *0.170* | *3.28* | *−1.94* |
| H(4)···C(6A) | 3.244 | −0.312 | −0.194 | 0.011 | 0.168 | 3.22 | −1.87 |
| *(−x + 1, −y, −z)* | *3.244* | *−0.319* | *−0.194* | *0.015* | *0.188* | *3.70* | *−2.28* |
| H(6A)···C(1) | 3.381 | 0.117 | −0.331 | 0.005 | 0.110 | 2.04 | −1.09 |
| *(x + 1, y, z)* | *3.389* | *0.026* | *−0.339* | *0.007* | *0.117* | *2.20* | *−1.22* |
| H(6)···C(7A) | 3.382 | 0.312 | −0.332 | 0.005 | 0.175 | 3.22 | −1.68 |
| *(x − 1, y − 1, z)* | *3.269* | *0.072* | *−0.218* | *0.013* | *0.194* | *3.75* | *−2.21* |
| H(6)···C(1A) | 3.409 | 0.109 | −0.359 | 0.006 | 0.107 | 2.00 | −1.1 |
| *(x − 1, y − 1, z)* | *3.398* | *0.034* | *−0.348* | *0.006* | *0.114* | *2.13* | *−1.16* |
| H(5A)···C(1A) | 3.726 | 0.376 | −0.676 | 0.005 | 0.106 | 1.97 | −1.05 |
| *(x, y − 1, z)* | *3.60* | *0.302* | *−0.550* | *0.006* | *0.123* | *2.30* | *−1.24* |
| H(7A)···C(1) | 3.835 | −0.373 | −0.785 | 0.006 | 0.074 | 1.41 | −0.8 |
| *(−x + 1, −y + 1, −z)* | *3.842* | *−0.390* | *−0.792* | *0.005* | *0.070* | *1.32* | *−0.73* |
| C(10)···C(8A) | 3.337 | 0.049 | 0.363 | 0.032 | 0.348 | 7.33 | −5.18 |
| *(−x + 1, −y + 1, −z)* | *3.342* | *−0.108* | *0.358* | *0.030* | *0.309* | *6.52* | *−4.62* |
| C(3)···C(8) | 3.366 | 0.068 | 0.334 | 0.038 | 0.310 | 6.97 | −5.5 |
| *(−x + 1, −y, −z)* | *3.382* | *0.087* | *0.318* | *0.040* | *0.398* | *8.69* | *−6.54* |
| C(6)···C(10) | 3.380 | −0.103 | 0.320 | 0.024 | 0.295 | 5.98 | −3.93 |
| *(−x + 1, −y, −z)* | *3.383* | *−0.056* | *0.317* | *0.042* | *0.354* | *8.02* | *−6.39* |
| C(3A)···C(8A) | 3.386 | 0.109 | 0.314 | 0.036 | 0.330 | 7.22 | −5.45 |
| *(−x + 2, −y + 1, −z + 1)* | *3.384* | *−0.050* | *0.316* | *0.032* | *0.315* | *6.73* | *−4.88* |
| C(6A)···C(10A) | 3.400 | −0.113 | 0.300 | 0.026 | 0.270 | 5.62 | −3.88 |
| *(−x + 2, −y + 1, −z + 1)* | *3.409* | *−0.113* | *0.291* | *0.033* | *0.242* | *5.46* | *−4.32* |
| C(2A)···C(5A) | 3.498 | −0.010 | 0.202 | 0.030 | 0.336 | 7.01 | −4.86 |
| *(−x + 2, −y + 1, −z + 1)* | *3.633* | *−0.008* | *0.067* | *0.037* | *0.342* | *7.49* | *−5.68* |
| C(1)···C(4) | 3.503 | 0.079 | 0.197 | 0.028 | 0.260 | 5.53 | −3.98 |
| *(−x + 1, −y, −z)* | *3.567* | *0.015* | *0.133* | *0.037* | *0.348* | *7.60* | *−5.73* |
| C(2)···C(4) | 3.609 | 0.069 | 0.091 | 0.029 | 0.300 | 6.30 | −4.44 |
| *(−x + 1, −y, −z)* | *3.678* | *−0.097* | *0.021* | *0.037* | *0.348* | *7.60* | *−5.73* |
| C(10A)···C(11A) | 3.817 | 0.534 | −0.117 | 0.039 | 0.306 | 6.96 | −5.58 |
| *(−x + 1, −y + 2, −z + 1)* | *3.778* | *0.215* | *−0.078* | *0.026* | *0.214* | *4.60* | *−3.37* |
| O(1A)···C(3) | 3.405 | −0.364 | −0.015 | 0.021 | 0.350 | 6.86 | −4.18 |
| *(−x + 1, −y + 1, −z)* | *3.391* | *−0.302* | *−0.001* | *0.021* | *0.344* | *6.75* | *−4.12* |
| O(1)···C(5) | 3.466 | −0.071 | −0.076 | 0.030 | 0.369 | 7.61 | −5.16 |
| *(x, y + 1, z)* | *3.469* | *0.056* | *−0.079* | *0.034* | *0.399* | *8.36* | *−5.85* |
| O(1A)···C(5A) | 3.475 | −0.043 | −0.085 | 0.030 | 0.375 | 7.72 | −5.22 |
| *(x, y + 1, z)* | *3.465* | *0.064* | *−0.075* | *0.034* | *0.407* | *8.51* | *−5.93* |
| O(1)···C(11) | 3.556 | 0.031 | −0.166 | 0.029 | 0.203 | 4.54 | −3.56 |
| *(−x + 1, −y + 1, −z)* | *3.438* | *−0.009* | *−0.048* | *0.032* | *0.386* | *8.02* | *−5.52* |
| O(1A)···C(11A) | 3.631 | 0.133 | −0.241 | 0.035 | 0.187 | 4.57 | −4.04 |
| *(−x + 2, −y + 2, −z + 1)* | *3.506* | *0.036* | *−0.116* | *0.031* | *0.362* | *7.53* | *−5.2* |
| | | | Form B | | | | |
| H(3)···O(3) | 2.354 | 0.131 | 0.386 | 0.061 | 1.091 | 22.77 | −15.82 |
| *(−x + 2, −y + 3, −z)* | *2.362* | *0.109* | *0.378* | *0.058* | *1.036* | *21.53* | *−14.84* |
| H(7)···O(2) | 2.386 | 0.213 | 0.354 | 0.041 | 1.035 | 20.32 | −12.45 |
| *(−x + 1, −y + 1, −z)* | *2.382* | *0.121* | *0.358* | *0.055* | *1.016* | *20.94* | *−14.2* |
| H(4)···O(3) | 2.546 | 0.104 | 0.194 | 0.038 | 0.731 | 14.62 | −9.32 |
| *(−x + 2, −y + 3, −z)* | *2.538* | *0.109* | *0.202* | *0.038* | *0.705* | *14.14* | *−9.09* |
| C(4)···C(8) | 3.551 | −0.022 | 0.149 | 0.032 | 0.341 | 7.20 | −5.11 |
| *(x, y + 1, z)* | *3.531* | *−0.040* | *0.169* | *0.048* | *0.385* | *8.97* | *−7.46* |
| C(5)···C(7) | 3.562 | −0.149 | 0.138 | 0.03 | 0.346 | 7.19 | −4.95 |
| *(x, y + 1, z)* | *3.549* | *−0.035* | *0.151* | *0.045* | *0.38* | *8.68* | *−7.01* |
| O(1)···C(2) | 3.300 | −0.326 | 0.09 | 0.038 | 0.489 | 10.22 | −7.13 |
| *(x, y − 1, z)* | *3.479* | *−0.094* | *−0.089* | *0.021* | *0.263* | *5.28* | *−3.39* |
| O(1)···C(11) | 3.516 | −0.151 | −0.126 | 0.016 | 0.266 | 5.15 | −3.05 |
| *(−x + 3/2, y − 1/2, −z + 1/2)* | *3.301* | *−0.252* | *0.089* | *0.040* | *0.542* | *11.30* | *−7.85* |

[a] The values from periodic calculation are given in italics. The symmetry codes are given in the second row under each interaction
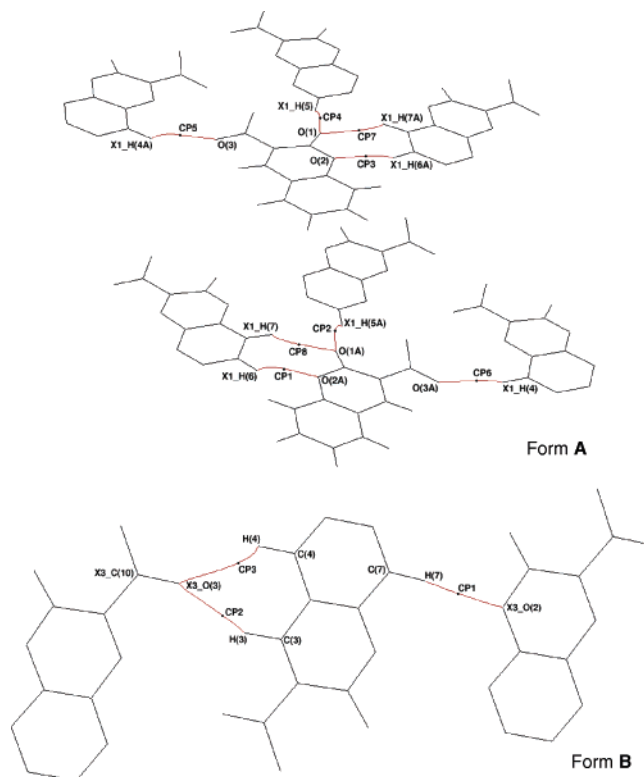
**Figure 3.** Bond path character showing the BCP locations along the C−H···O interaction lines shown in red.

Mapping of the charge density distribution in the intermolecular interaction region, molecular electrostatic potential surface, estimation of the intermolecular interaction energy density,[16,19,47] and finally a description of the lattice energy from experimental and theoretical analysis would provide relevant parameters to distinguish between Form A and Form B. Table 3 list the intermolecular interactions in terms of the interaction line $R_{ij}$, the value of interpenetration of van der Waals spheres of the donor and acceptor atoms[16,20,44] [$(\Delta r_D + \Delta r_A)$ and $(\Delta r_D − \Delta r_A)$], the value of $\rho_b(\mathbf{r})$, and $\nabla^2 \rho_b(\mathbf{r})$ along with the $G(\mathbf{r}_{CP})$ and $V(\mathbf{r}_{CP})$ energy density for each interaction from both experiment and theory. It is to be noted that intermolecular interactions involving H atoms of the −CH$_3$ group are not included. Apart from the interactions identified in Form A earlier,[13] an additional pair of
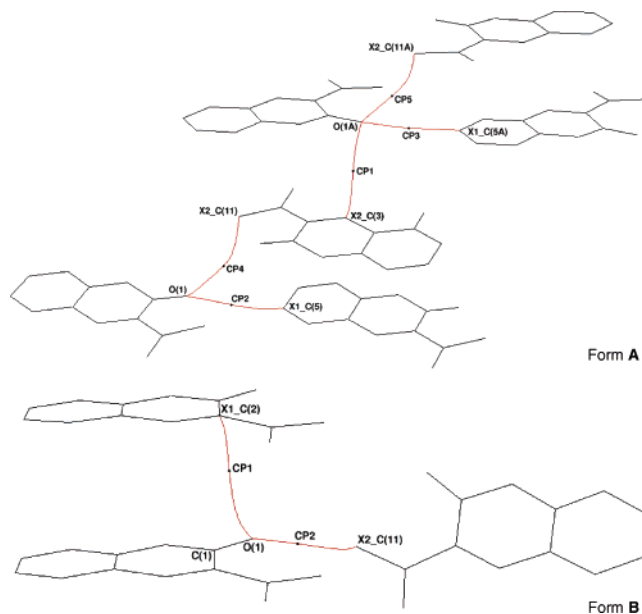


**Figure 4.** Bond path character showing the critical point locations along the C=O···C$_\pi$ interaction lines.

C−H···O hydrogen bonds and several C−H···C$_\pi$ and C$_\pi$···C$_\pi$ intermolecular interactions could be identified based on these calculations. On the other hand, Form B generates only three C−H···O hydrogen bonds and two C$_\pi$···C$_\pi$ intermolecular interactions with no C−H···C$_\pi$ interaction. The values of the density related parameters listed in Table 3 depict the nature, strength, and directionality of intermolecular interactions in particular characterizing hydrogen-bonded regions and pure van der Waals regions. To gain further insights into features resulting in the two polymorphs BPs and the corresponding Laplacian maps in selected regions have been analyzed (Figures 3−7). The dimeric and bifurcated nature of C−H···O interactions in terms of BPs and associated BCPs in both forms are easily distinguishable from Figure 3. It is noteworthy that atom O(1) of Form B has no C−H···O interaction; however, BCPs in both forms are found in the region representing C=O···C$_\pi$ type of features[48,49] (Figure 4). It is also interesting to note that in Form A the BP of C=O···C$_\pi$ points toward the O atom, while in Form B the BP points either to the center of C=O bond or to

**Table 4. (a) Binding Energies, (b) Molecular Relaxation Energies, and (c) Lattice Energies**

(a) Binding Energies

| | XDINTER | | CRYSTAL03 | CRYSTAL03 |
| | experimental | | HF/6-31G** | B3LYP/6-31G** |
| crystal | URMM | KRMM | | |
|---|---|---|---|---|
| Form A (kJ/2mol) | −299.2 | −224.2 | −11.0 | −46.1 |
| Form B (kJ/mol) | −110.2 | −90.3 | −3.5 | −18.7 |

(b) Molecular Relaxation Energies

| molecule | GAUSSIAN98 HF/6-31G** | GAUSSIAN98 B3LYP/6-31G** |
|---|---|---|
| Form A (kJ/2mol) | −74.5 | −52.0 |
| Form B (kJ/mol) | −18.8 | −11.6 |

(c) Lattice Energies

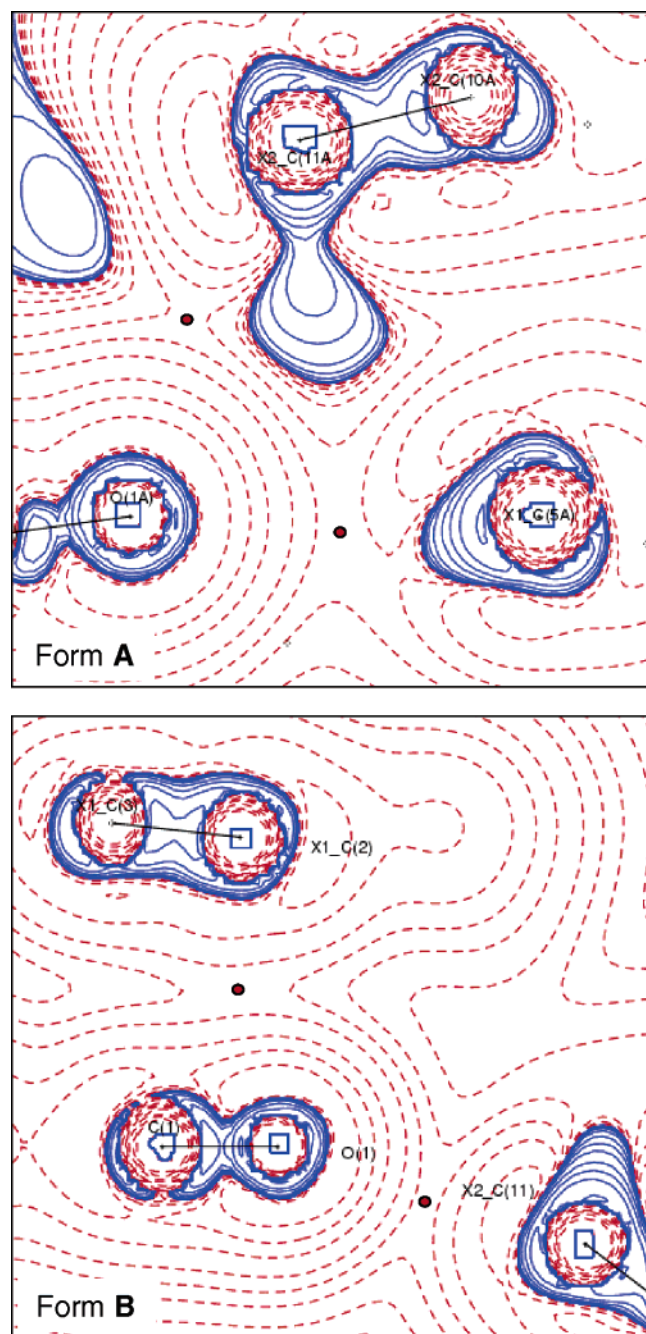| | experimental (XDINTER) | | | | HF/6-31G** (CRYSTAL03) | B3LYP/6-31G** (CRYSTAL03) |
| | URMM | | KRMM | | | |
| crystal | HF | DFT | HF | DFT | | |
|---|---|---|---|---|---|---|
| Form A (kJ/2mol) | −224.6 | −247.2 | −149.7 | −172.2 | 63.5 | 5.9 |
| Form B (kJ/mol) | −91.4 | −98.6 | −71.5 | −78.7 | 15.3 | −7.1 |

**Figure 5.** Laplacian [$\nabla^2\rho_b(\mathbf{r})$] of a representative C=O⋯$C_\pi$ intermolecular interaction. All the Laplacian maps are drawn at logarithmic intervals in $-\nabla^2\rho_b$ e Å$^{-5}$; solid blue and broken red lines represent positive and negative contours, respectively.



**Figure 6.** Bond path character showing the critical point locations along the $C_\pi$⋯$C_\pi$ interaction lines.

the O atom (Figure 5). However, the $C_\pi$⋯$C_\pi$ interactions (Figures 6 and 7) are directed to the center of the bond. The subtle differences seen qualitatively bring out the details of packing polymorphism in 3-acetylcoumarin. These observations also suggest that Form A with a reasonably large number, 31 in all, of weak intermolecular interactions compared to Form B (seven interactions) would indeed be a thermodynamically stable form. However, this conclusion is only qualitative unless the interaction energies and corresponding effect on lattice energies in the two forms are calculated.

The lattice energies are estimated both from experimental and theoretical approaches. The experimental results are compared with those from both the HF and DFT (B3LYP) calculations. Table 4a lists the bindi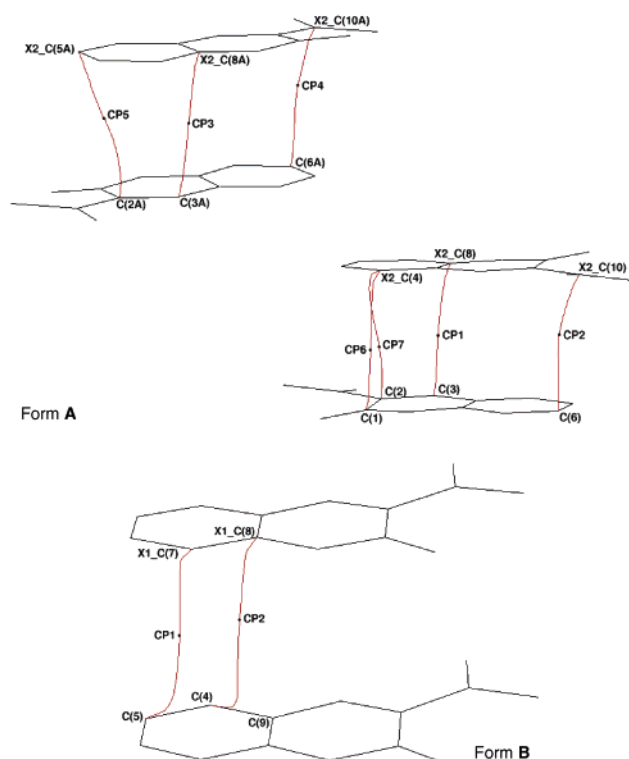ng energies calculated from multipole refinements based on the unrestricted multipole model (URMM)[50] and $\kappa'$-restricted multipole model (KRMM)[50] and the values obtained via CRYSTAL03 from both HF and DFT approaches. Since Form A contains two independent molecules in the asymmetric unit the values given are always for the (dimer) asymmetric unit.[15] The experimental results show a dominant contribution to the binding energy from the dispersion term (−369.8 kJ/2mol), with the exchange-repulsion term and the electrostatic term being 400.4 kJ/2mol and −329.8 kJ/2mol, respectively. For Form B as well the dispersion term dominates with a value of −168.6 kJ/mol with the exchange-repulsion term and the electrostatic term being 168.2 kJ/mol and −109.8 kJ/mol, respectively. It is observed that the binding energies from DFT calculations via CRYSTAL03 are significantly lower than that obtained from HF calculations. It is to be noted that in contrast to the electrostatic interactions, dispersion interactions (strong in aromatic systems) are always attractive.[33a,51] The dispersion energy term is of extreme importance, particularly in the case of aromatic systems as can be seen from the recent study on 2-amino-5-nitropyridine and 2-amino-5-nitro-1,3-pyridine,[52] p-benzoquinone,[53] and p-amino-p′-nitrobiphenyl.[51] The relaxation energies (Table 4b) are generated based on a gas phase calculation by GAUSSIAN98 using HF and B3LYP levels with the 6-31G** basis set, and Table 4c shows the comparison of the lattice energies based on the values obtained from binding and relaxation energies for both forms. The energies calculated based on URMM are lower in general compared to that of KRMM. It is to be noted that even though the magnitudes do not match, the results bring out clearly that the lattice energy for the dimer of Form A (e.g., −172.2 kJ/2mol from KRMM/DFT) is lower than that of the monomer of Form B (−78.7 kJ/mol). In fact, if one looks at a single molecule of Form A the lattice energy would be about −86.1 kJ/mol, which clearly brings out the cause of the occurrence of concomitant polymorphism (nearly equivalent crystal energet-
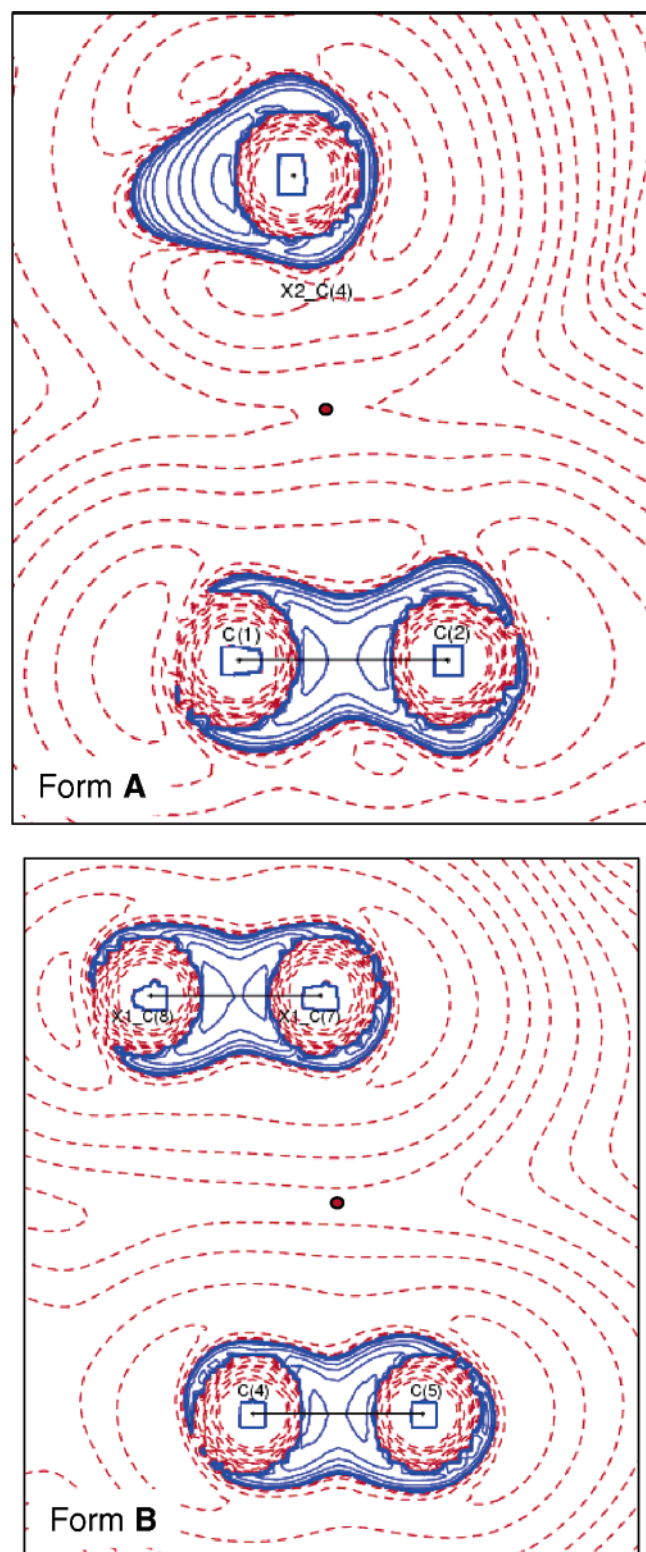
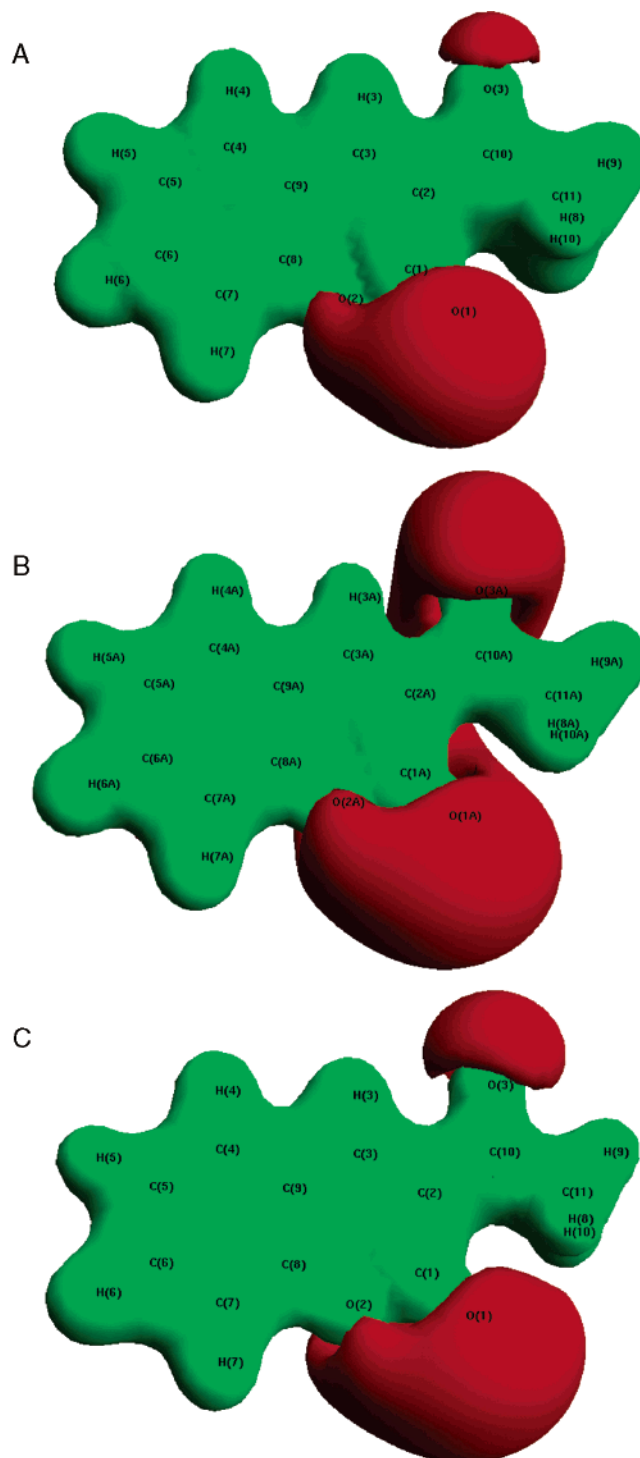**Figure 7.** Laplacian [$\nabla^2 \rho_b(\mathbf{r})$] of a representative $C_\pi \cdots C_\pi$ intermolecular interaction.



**Figure 8.** (A) Molecular electrostatic potential in molecule 1 of Form A. The potential of $+0.30$ e Å$^{-1}$ is shown as the green isosurface, while $-0.15$ e Å$^{-1}$ is shown as the red isosurface in all the maps. (B) Molecular electrostatic potential in molecule 2 (Form A) of 3-acetylcoumarin. (C) Molecular electrostatic potential in Form B of 3-acetylcoumarin.

ics). This is in agreement with the results obtained from the analysis of intermolecular interactions, which showed that Form A is the thermodynamically preferred form. The corresponding values from theory (DFT) appear repulsive or slightly attractive mainly due to the neglect of dispersion energies in these calculations. Further, the HF method generally shows a destabilization due to the absence of a contribution from electron correlation. Similar observations were noticed in the case of

*p*-nitroaniline[33a,51] and *p*-amino-*p*′-nitrobiphenyl[51] studied by Abramov et al.

Plotting of molecular surfaces such as space-filling models, van der Waals surfaces, and electron density isosurfaces show features of how molecules fill space, but none allows for deformation of the molecular space in the crystalline environment.[54] Analysis of electrostatic potential on the molecular surface originally developed for theoretical data[55] has been

applied to experimental data to gain insights into drug receptor interactions in recent times.[9] Thus, molecular electrostatic potential maps (Figure 8), which carry a wealth of qualitative and quantitative information, also bring out the effect of the crystalline environment and effectively point to the differences in both Form A and Form B. Both polymorphs possess large electropositive surfaces, which also explains the observed large molecular dipole moment values exhibited. However, the electronegative areas, varying each case, are separated from the electropositive areas, and in molecule 2 of Form A the electronegative area loops around the electropositive area. It is to be noted that the O atom [O(1)] in molecule 2 of Form A displays a large electronegative region, indicating its involvement in generating several interactions (Figure 4) compared to molecule 1 of Form A and that of Form B.

## Conclusion

This study for the first time brings out the differences in concomitant polymorphs in terms of (i) experimental electron densities, (ii) theoretical electron densities, (iii) topology of intermolecular interactions, (iv) interaction energies (lattice energies), and (v) electrostatic potential maps. The use of low-temperature high-resolution single-crystal X-ray diffraction experiments on one hand to derive charge densities and the comparison of charge densities and topological parameters derived from such experiments with values obtained from theoretical calculation on the other clearly demonstrate the utility of charge densities to distinguish between concomitant polymorphs. Identification of weak intermolecular interactions based purely on distance−angle criteria hence is inadequate and in the context of "quantitative crystal engineering" recognition of critical points in terms of charge density distribution becomes extremely relevant to justify the occurrence of any interaction in the intermolecular space. In the context of polymorphic drugs, this approach is expected to provide useful inputs for "drug design" and characterization of all possible polymorphs.

**Supporting Information Available:** (i) Residual density maps and dynamic deformation density maps, (ii) multipole population coefficients, $\kappa$ and $\kappa'$ values obtained from the multipole refinement and definitions of local axes, and (iii) crystallographic information files (CIF) for Form A and Form B. This material is available free of charge via the Internet at http://pubs.acs.org.

## References

(1) Bernstein, J. *Prog. Clin. Biol. Res*. **1989**, *289*, 203-215. Brittain, H. G. *Polymorphism in Pharmaceutical Solids*; Marcel Dekker: New York, 1999; Vol. 95.

(2) Bernstein, J. *Polymorphism in Molecular Crystals*; Oxford University Press: Oxford, Great Britain, 2002.

(3) Allen, F. H. *Acta Crystallogr. B* **2002**, *58*, 380−388. Allen, F. H.; Motherwell, W. D. S. *Acta Crystallogr. B* **2002**, *58*, 407−422. CSD (Version 5.25, November 2003 and three updates til July 2004) reports 322 421 structures of which only 5813 contain qualify the word "polymorph" while searching for "organic" molecules only. Among these, only 138 are with space group $P\bar{1}$ ($Z = 4$, $Z' = 2$) and 383 are with space group $P2_1/n$ ($Z = 4$, $Z' = 1$). A total of 82 polymorphs are reported as a combination of $P\bar{1}$ and $P2_1/n$ out of which only 12 are reported as a combination of $P\bar{1}$ ($Z = 4$, $Z' = 2$)

and $P2_1/n$ ($Z = 4$, $Z' = 1$). It is of interest to note that there is only one reported example (CSD Refcode: HAZFAP, 4, 4′-bipyridinium salt of squaric acid; Reetz, M.T.; Höger, S.; Harms, K. *Angew. Chem., Int. Ed. Engl.* **1994**, *33*, 181−183.), which is concomitant.

(4) Vrcelj, R. M.; Gallagher, G. H.; Sherwood, J. N. *J. Am. Chem. Soc.* **2001**, *123*, 2291−2295. Davey, R. J.; Blagden, N.; Righini, S.; Alison, H.; Quayle, M. J.; Fuller, S. *Cryst. Growth Des.* **2001**, *1*, 59−65 and references therein.

(5) Bernstein, J.; Davey, R. J.; Henck, J.-O. *Angew. Chem., Int. Ed. Engl.* **1999**, *38*, 3440−3461.

(6) Reed, S. M.; Weakley, T. J. R.; Hutchison, J. E. *Cryst. Eng.* **2000**, *3*, 85−99.

(7) Coppens, P. *X-ray Charge Densities and Chemical Bonding*; Oxford University Press: Oxford, 1997.

(8) Hohenberg, P.; Kohn, W. *Phys. Rev. B* **1964**, *136*, 864−871.

(9) Overgaard, J.; Hibbs, D. E. *Acta Crystallogr. A* **2004**, *60*, 480−487.

(10) Kulkarni, G. U.; Kumaradhas, P.; Rao, C. N. R. *Chem. Mater.* **1998**, *10*, 3498−3505.

(11) Gopalan, R. S.; Kulkarni, G. U.; Rao, C. N. R. *ChemPhysChem* **2000**, *1*, 127−135.

(12) Whitten, A. E.; Dittrich, B.; Spackman, M. A.; Turner, P.; Brown, T. C. *Dalton Trans.* **2004**, 23−29.

(13) Munshi, P.; Venugopala, K. N.; Jayashree, B. S.; Guru Row, T. N. *Cryst. Growth Des.* **2004**, *4*, 1105−1107.

(14) Pichon-Pesme, V.; Lecomte, C. *Acta Crystallogr. Sect. B* **1998**, *54*, 485−493. Overgaard, J.; Schiøtt, B.; Larsen, F. K.; Iversen, B. B. *Chem. Eur. J.* **2001**, *7*, 3756−3767. Hambley, T. W.; Hibbs, D. E.; Turner, P.; Howard, S. T.; Hursthouse, M. B. *J. Chem. Soc., Perkin Trans. 2* **2002**, 235−239. Gatti, C.; May, E.; Destro, R.; Cargnoni, F. *J. Phys. Chem. A* **2002**, *106*, 2707−2720.

(15) Overgaard, J.; Waller, M. P.; Platts, J. A.; Hibbs, D. E. *J. Phys. Chem. A* **2003**, *107*, 11201−11208.

(16) Munshi, P.; Guru Row, T. N. *J. Phys. Chem. A* **2005**, *109*, 659−672.

(17) Coppens, P. *Acta Crystallogr. A* **1998**, *54*, 779−788.

(18) Hansen, N. K.; Coppens, P. *Acta Crystallogr. A* **1978**, *34*, 909−921.

(19) Bader, R. F. W. *Atoms in Molecules: A Quantum Theory*; Oxford University Press: Oxford, U.K. 1990. Bader, R. F. W. *J. Phys. Chem. A* **1998**, *102*, 7314−7323.

(20) Koch, U.; Popelier, P. L. A. *J. Phys. Chem.* **1995**, *99*, 9747−9754. Popelier, P. *Atoms in Molecules. An Introduction*; Prentice Hall, UK, 2000; pp 150−153.

(21) (a) Bondi, A. *J. Phys. Chem.* **1964**, *68*, 441−451. (b) Nyburg, S. C.; Faerman, C. H. *Acta Crystallogr. B* **1985**, *41*, 274−279.

(22) Knoevenagel, F. *Ber. Dtsch. Chem. Ges.* **1898**, *31*, 732.

(23) Munshi, P.; Guru Row, T. N. *Acta Crystallogr. B* **2002**, *58*, 1011−1017. Munshi, P.; Guru Row, T. N. *Acta Crystallogr. B* **2003**, *59*, 159.

(24) Bruker. *SMART* (V5.628), *SAINT* (V6.45a), Bruker AXS Inc., Madison, WI, 2004.

(25) Blessing, R. H. *Crystallogr. Rev.* **1987**, *1*, 3−58.

(26) Sheldrick, G. M. *SHELXS97* and *SHELXL97*, program for crystal structure refinement; University of Göttingen, Germany, 1997.

(27) Farrugia, L. J. *WinGX*, Version 1.64.05. *J. Appl. Crystallogr.* **1999**, *32*, 837−838.

(28) Farrugia, L. J. *J. Appl. Crystallogr.* **1997**, *30*, 565.

(29) Nardelli, M. *J. Appl. Crystallogr.* **1995**, *28*, 569.

(30) Koritsanszky, T. S.; Howard, S.; Macchi, P.; Gatti, C.; Farrugia, L. J.; Mallinson, P. R.; Volkov, A.; Su, Z.; Richter, T.; Hansen, N. K. *XD* (version 4.10, July), a computer program package for multipole refinement and analysis of electron densities from diffraction data; Free University of Berlin, Germany; University of Wales, Cardiff, UK.; Università di Milano, U.K.; CNR-ISTM, Milano, U.K.; University of Glasgow, U.K.; State University of New York, Buffalo, USA.; University of Nancy, France, 2003.

(31) Clementi, E.; Roetti, C. *At. Data Nucl. Data Tables* **1974**, *14*, 177−478.

(32) Allen, F. H. *Acta Crystallogr. B* **1986**, *42*, 515−522.

(33) (a) Abramov, Y. A.; Volkov, A.; Wu, G.; Coppens, P. *Acta Crystallogr. A* **2000**, *56*, 585−591. (b) Kisiel, Z. PROSPE, Programs for ROtational SPEctroscopy, http://info.ifpan.edu.pl/~kisiel/prospe.htm.

(34) Spackman, M. A. *J. Chem. Phys.* **1986**, *38*, 6587−6601.

(35) Frisch, M. J.; Trucks, G. W.; Schlegel, H. B.; Scuseria, G. E.; Robb, M. A.; Cheeseman, J. R.; Zakrzewski, V. G.; Montgomery, J. A., Jr.; Stratmann, R. E.; Burant, J. C.; Dapprich, S.; Millam, J. M.; Daniels, A. D.; Kudin, K. N.; Strain, M. C.; Farkas, O.; Tomasi, J.; Barone, V.; Cossi, M.; Cammi, R.; Mennucci, B.; Pomelli, C.;

Adamo, C.; Clifford, S.; Ochterski, J.; Petersson, G. A.; Ayala, P. Y.; Cui, Q.; Morokuma, K.; Malick, D. K.; Rabuck, A. D.; Raghavachari, K.; Foresman, J. B.; Cioslowski, J.; Ortiz, J. V.; Stefanov, B. B.; Liu, G.; Liashenko, A.; Piskorz, P.; Komaromi, I.; Gomperts, R.; Martin, R. L.; Fox, D. J.; Keith, T.; Al-Laham, M. A.; Peng, C. Y.; Nanayakkara, A.; Gonzalez, C.; Challacombe, M.; Gill, P. M. W.; Johnson, B.; Chen, W.; Wong, M. W.; Andres, J. L.; Gonzalez, C.; Head-Gordon, M.; Replogle, E. S.; Pople, J. A. *GAUSSIAN 98*; Gaussian, Inc.: Pittsburgh, PA, 1998.

(36) Abramov, Y. A.; Volkov, A.; Wu, G.; Coppens, P. *J. Phys. Chem. B* **2000**, *104*, 2183−2188.

(37) Saunders, V. R.; Dovesi, R.; Roetti, C.; Causa, M.; Harrison, N. M.; Orlando, R.; Zicovich-Wilson, C. M. *CRYSTAL03 1.0 User's Manual*; University of Torino and CCLRC, 2003.

(38) Becke, A. D. *J. Chem. Phys.* **1993**, *98*, 5648−5652. Lee, C.; Yang, W.; Parr, R. G. *Phys. Rev. B* **1988**, *37*, 785−789.

(39) Hariharan, P. C.; Pople, J. A. *Theor. Chim. Acta* **1973**, *28*, 213−222.

(40) Oddershede, J.; Larsen, S. *J. Phys. Chem. A* **2004**, *108*, 1057−1063.

(41) Spackman, M. A.; Mitchell, A. M. *Phys. Chem. Chem. Phys.* **2001**, *3*, 1518−1523.

(42) Boys, S. F.; Bernardi, F. *Mol. Phys.* **1970**, *19*, 553−566.

(43) Hirshfeld, F. L. *Acta Crystallogr. A* **1976**, *32*, 239−244.

(44) Mallinson, P. R.; Smith, G. T.; Wilson, C. C.; Grech, E.; Woz'niak, K. *J. Am. Chem. Soc.* **2003**, *125*, 4259−4270.

(45) Hibbs, D. E.; Overgaard, J.; Piltz, R. O. *Org. Biomol. Chem.* **2003**, *1*, 1191−1198.

(46) May, E.; Destro, R.; Gatti, C. *J. Am. Chem. Soc.* **2001**, *123*, 12248−12254 and the references therein.

(47) Abramov, Y. A. *Acta Crystallogr. A* **1997**, *53*, 264−272. Espinosa, E.; Molins, E.; Lecomte, C. *Chem. Phys. Lett.* **1998**, *285*, 170−173.

(48) Moorthy, J. N.; Samant, S. D.; Venkatesan, K. *J. Chem. Soc., Perkin Trans. 2* **1994**, 1223−1228.

(49) Yang, X.; Wu, D.; Ranford, J. D.; Vittal, J. J. *Cryst. Growth Des.* **2005**, *5*, 41−43 and the references therein.

(50) Abramov, Y. A.; Volkov, A.; Coppens, P. *Chem. Phys. Lett.* **1999**, *311*, 81−86.

(51) Abramov, Y. A.; Volkov, A.; Coppens, P. *J. Mol. Struct. (THEO-CHEM)* **2000**, *529*, 27−35.

(52) Stone, A. J.; Tsuzuki, S. *J. Phys. Chem. B* **1997**, *101*, 10178−10183.

(53) Cárdenas-Jirón, G. I.; Masunov, A.; Dannenberg, J. J. *J. Phys. Chem. A* **1999**, *103*, 7042−7046.

(54) McKinnon, J. J.; Spackman, M. A.; Mitchell, A. S. *Acta Crystallogr. B* **2004**, *60*, 627−668.

(55) Politzer, P.; Murray, J. S. *Theo. Chem. Acc.* **188**, 134−142.